European Journal of Chemistry

View Journal Online
View Article Online

Response surface methodology optimization and modeling of green synthesis conditions for TiO_2-ZnO nanocomposites using *Vigna unguiculata* L. extract

Auwal Yusha'u *, Kamaluddeen Suleiman Kabo and Siaka Abdulfatai Adabara

Department of Chemistry, Faculty of Physical Sciences, Federal University Dutsin-Ma, P.M.B. 5001, Katsina State, Nigeria

* *Corresponding author at: Department of Chemistry, Faculty of Physical Sciences, Federal University Dutsin-Ma, P.M.B. 5001, Katsina State, Nigeria.*
e-mail: auwalyushau2018@gmail.com (A. Yusha'u).

RESEARCH ARTICLE

10.5155/eurjchem.16.2.154-168.2670

Received: 10 February 2025
Received in revised form: 7 March 2025
Accepted: 9 April 2025
Published online: 30 June 2025
Printed: 30 June 2025

KEYWORDS

Active sites
Optimization
Box-Behnken design
Vigna unguiculata L. extract
Response surface methodology
Titania-zinc oxide nanocomposite

ABSTRACT

Developing a more efficient and sustainable method than conventional chemical and physical approaches to synthesize TiO_2-ZnO nanocomposites is essential to reduce environmental impact. Green synthesis offers a sustainable alternative, minimizing toxic solvents and utilizing renewable biological sources. TiO_2-ZnO NCs is a well-known binary nanocomposite with different potential biomedical, photocatalysis and solar cell applications due to its excellent physiochemical properties. This study presents the response surface methodology, optimization, and modeling of the reaction conditions of TiO_2-ZnO NCs by green synthesis using the co-precipitation method from *Vigna unguiculata* L. extract as a reducing and stabilizing agent. Optimization of independent reaction conditions such as amount of dopant, reaction temperature, initial pH, and stirring time was performed using Response Surface Methodology-Box Behnken Design (RSM-BBD) of the design expert version 13 software (DX13). The strength and amount of active site of the synthesized TiO_2-ZnO NCs were calculated by back titration analysis. The results show that TiO_2-ZnO NCs were successfully precipitated and the optimization study obtained shows that the optimum number of active sites (8.881 mmol/g) of the TiO_2-ZnO NCs was achieved at 10.00% MR of TiO_2, 90 °C reaction temperature, initial pH of 11 and 23 min stirring time. The optimal reaction conditions were supported and confirmed by the solution ramp functions and bar graph plots. Statistically, the regression model and analysis of variance (ANOVA) revealed that the initial pH was the most significant parameter among the selected reaction conditions with the probability value (*p*-values) of 0.0011. The two-dimensional (2D) contour and three-dimensional (3D) response surface plots demonstrated a good interaction between the reaction variables during the biosynthesis. The porosity, particle size distribution (PSD) and specific surface area (SSA) of optimized TiO_2-ZnO NCs were evaluated using the nonlinear density functional theory (NLDFT) method. Consequently, the pore volume, pore size and SSA for the developed TiO_2-ZnO NCs were found to be 5.45×10^{-2} cm^3/g, 3.23 nm, and 351.80 m^2/g, respectively, indicating that the optimized TiO_2-ZnO NCs are mesoporous in nature. This work indicated that mesoporous TiO_2-ZnO NCs were prepared through the novel use of *Vigna unguiculata* L. extract. RSM-BBD was successfully used in the design of experiment, model development, and optimization of highly active TiO_2-ZnO NCs production.

Cite this: *Eur. J. Chem.* **2025**, *16(2)*, 154-168 **Journal website**: www.eurjchem.com

1. Introduction

Recently, nanotechnology has become a popular and promising field of technology that has attracted the attention and interests of many researchers, scholars, and engineers around the world, this is due to its advantages over the other field of sciences [1,2]. Some of the major applications of nanotechnology include photocatalysis [3], fuel cells [4], photovoltaic cells [5], sensors [6], and optical and thermal applications [7]. This technology involves the use of very small particle size, usually ranging from 1-100 nm [8,9], and thus includes semiconducting materials. Some of the common examples of semiconducting nanomaterials include ZnO, TiO_2, ZrO_2, ZnS, Fe_2O_3, WO_3, ZrS [8-10]. Zinc oxide (ZnO) and titanium dioxide (TiO_2) NPs are widely used as photocatalysts due to their availability in nature, being inexpensive, chemical stability, and being environmental friendly species [11]. ZnO has three crystal structures; hexagonal wurtzite, cubic rock salts, and cubic zinc blend. The most common is the wurtzite structure, as it is the most stable under ambient conditions. The wurtzite structure has two crystal lattice parameters, $a = b =$ 3.2495 Å, c =5.2069 Å and and the c/a ratio is 1.60 [12]. On the other hand, TiO_2 NP has many different types of crystal structure known as polymorphs [13]. The most important and common phases of TiO_2 NP are found naturally as rutile, anatase, and brookite. However, among these crystal structures, only anatase and rutile have been widely applied for photocatalysis due to their ability to harness photons of light during photocatalytic reactions [14].

ISSN 2153-2249 (Print) / ISSN 2153-2257 (Online)
https://dx.doi.org/10.5155/eurjchem.16.2.154-168.2670

Information from the literature revealed that both TiO_2 and ZnO NPs suffered from a certain number of drawbacks when applied individually for photocatalytic activity. First, TiO_2 (anatase) and ZnO have wide bands of about 3.20 and 3.27 eV, respectively, which limits their use of the solar spectrum to only ultraviolet (UV) light, yet it accounts for only less than 3-5% of solar radiation [15]. Second, both TiO_2 and ZnO NPs have a high electron-hole pair recombination rate, resulting in reduced photodegradation [16]. Furthermore, it is notable that TiO_2 faces a problem of photocorrosion through self-oxidation, reducing its photostability [17,18]. Therefore, there is need to develop a new band gap modification approach that will improve the activity of the individual TiO_2 and ZnO NPs.

Different band gap modification methods such as doping, ion impregnation, dye sensitization, and coupling have been used with the aim of enhancing the morphology and photocatalytic activity of TiO_2 and ZnO NP [19-21]. However, the coupling method showed significant success over other modification methods [22] and was adopted in the present work. The process involves the mixing of two or more pure semiconductors (TiO_2 and ZnO NPs) together to improve their activity, reduce their band gap, and suppress the rate of recombination of the photogenerated electron-hole pair than the individual TiO_2 and ZnO NPs [23]. Various chemical and physical processes such as solvothermal, hydrothermal, mechanochemical, precipitation, sol-gel, co-precipitation, and green methods have been widely used for the synthesis of TiO_2-ZnO NCs [24-29]. Today, green synthesis is preferred because of its less time consumption, low cost, and use of biological sources, which do not require hazardous chemicals and sophisticated instrumentations during synthesis. Green synthesis deals with the preparation of nanomaterials (in this case, TiO_2- ZnO NC) from the extracts of biological sources such as plants, fruits, flowers, leaves, algae, fungi, bacteria, yeasts, *etc*. [30]. Green synthesis is also known as biosynthesis because it involves the use of biological sources extract. Plant extracts, in particular, offer great promise for biosynthesis due to their widespread availability, affordability, ease of use, and scalability [31,32]. Recently, various extracts of biological sources have been used as a reducing agent and stabilizing agent for the biosynthesis of TiO_2-ZnO nanocomposites [33]. Rusman *et al.* [34] investigated the green synthesis of ZnO/TiO_2 at different calcination temperatures 500, 600, 700 and 800 °C using *Calopogonium mucunoides* leaf extract as reducing and stabilizing agents. Similarly, Kelesoglu *et al.* [35] studied the green synthesis and structural characterization of ZnO nanoparticles and ZnO@TiO_2 nanocomposites using *cinnamomum verum* bark extract as a biogenic reducing agent and the results demonstrated significant success. Haghighizadeh *et al.* [36] reported the green synthesis of ZnO-TiO_2 nanophotocatalyst doped Fe (III) ions using bitter olive extract to treat textile wastewater containing reactive dyes and the results revealed a significant response. Similarly, Atiek *et al.* [37] reported the green synthesis of the TiO_2-ZnO hetero-structure using *Urtica smensis* leaf extract for antibacterial activity and the finding showed a good response. Furthermore, Bognar *et al.* [38] investigated sustainable green water nanotechnologies: the synthesis of nanoparticles from renewable sources and the results demonstrated significant responses.

Optimization is a process of finding the best conditions using the response surface methodology (RSM) of design expert (DX) software [39-41]. RSM consists of different tools such as Box Behnken Design (BBD), Face Central Composite Design (FCCD), Central Composite Design (CCD), and Taguchi array. Consequently, BBD are preferred due to their accuracy, less time consumption, and less number of runs in the design of experiment [42,43]. Nowadays, optimization processes are widely used to investigate the roles of variables and interactions among the parameters. Models like the quadratic function and the second-order interaction function are developed using the statistical table like the analysis of variance (ANOVA) and statistical regression equation [44,45]. Probability values (*p*-values) are mostly used to determine the contribution of each parameter studied [46]. A *p*-value < 0.05 indicates that the parameter is significant, while a *p*-value > 0.05 suggests that the variable is not significant [47,48].

Several studies have been conducted to optimize conditions, enhance nanoparticle yield, and improve commercial viability [49]. Traditionally, the optimization process was conducted using the classical method by changing an independent variable and fixing other variables. However, the shortcomings of the method are that it is time consuming and arduous and does not consider the interaction between the variables [50,51]. Recently, RSM has been applied to optimize reaction conditions for the synthesis of ZnO and TiO_2 and works by evaluating the interactions between variables and releasing the desired optimal conditions based on conducting several experiments [52,53].Rakhmanova *et al.* [54] reported the application of response surface methodology using Box Behnken Design for optimization of nanosized zinc oxide synthesis conditions such as applied voltage, tip-to-collectors distance, and annealing temperature on the size of ZnO particles by the electrospinning technique. The optimal conditions for the synthesis of ZnO were found at a constant applied potential of 16 kV, with a distance between the collector and nozzle of 12 cm, flow rate of 1 mL/h, and calcination temperature of 600 °C. Yusof *et al.* [55] investigated the optimization of the reaction conditions of the biosynthesis zinc oxide nanoparticles such as zinc concentration (200-500 mM), pH (6-10) and cell-free supernatant (CFS) volume ratio (20-50 %) using the desirability function-based response surface methodology. The optimal conditions for maximum yield and minimum particle size were found to be 2.47 g and 75.8 nm, respectively.

Several studies have focused on optimizing reaction conditions to enhance nanoparticle synthesis, photocatalytic efficiency, and biomedical applications. Mazloom *et al.* [56] optimized the synthesis of the $Zn_3V_2O_8$ nanostructure by adjusting parameters such as precursor type, reaction time, temperature, solvent and pH. Ghaedi *et al.* [57] utilized artificial neutral network partial swarm optimization (ANN-PSO) to optimize adsorption conditions, while Shaterian *et al.* [58] improved $LaMnO_3$-based photocatalysis. Raja *et al.* [59] optimized 4-chlorophenol photodegradation using Raschig rings-TiO_2 composites. Heydariyan *et al.* [60] improved electrochemical hydrogen storage by refining the synthesis conditions of $SmMn_2O_5/Mn_2O_3$/g-C_3N_4. Safardoust-Hojaghan *et al.* [61] optimized nitrogen-doped graphene quantum dots for bacterial detection. Diez-Orejas *et al.* [62] improved graphene oxide nanosheets for antimicrobial applications. Abdu *et al*. [63] and Sugiyama *et al.* [64] optimized photocatalytic degradation of pollutants, achieving significant results under optimal conditions.

Despite their abundance, bean leaves remain underutilized, mainly serving as a vegetable or food. *Vigna unguiculata* L., a member of the Fabaceae family along with *Phaseolus* species, plays a crucial role in nitrogen fixation. Although green synthesis of TiO_2-ZnO nanocomposites (NC) using various biological extracts has been reported, its synthesis from the *Vigna unguiculata* L. extract remains unexplored. Furthermore, the optimization of reaction conditions for this biosynthesis has not been investigated. In this study, TiO_2-ZnO NCs were synthesized via the co-precipitation method using *Vigna unguiculata* L. extract, with reaction parameters optimized and modeled through Response Surface Methodology-Box-Behnken Design (RSM-BBD) using DX13. Synthesized TiO_2-ZnO NCs demonstrate potential applications in biomedical, thermal, optical, photocatalytic and solar cell technologies [23].

Table 1. Level factorial Box Behken design for green synthesis of TiO_2-ZnO NCs

Parameter (Unit)	Notation	Low (codes)	Central (codes)	High (codes)
Amount of dopant (MW %)	A	1.00 (-1)	5.00 (0)	10.00 (+1)
Reaction temperature (°C)	B	85.00 (-1)	90.00 (0)	95.00 (+1)
Initial pH	C	4.00 (-1)	8.00 (0)	11.00 (+1)
Stirring time (min)	D	15.00 (-1)	20.00 (0)	30.00 (+1)

Figure 1. *Vigna unguiculata* L. plant.

2. Experimental

2.1. Chemicals

All of the chemicals used in this work were used as received from the manufacturers without further purification. These chemicals include zinc acetate dehydrate ($Zn(CH_3COO)_2{\cdot}2H_2O$, 98%) obtained from Sigma Aldrich, titanium acetate dehydrate ($Ti(NO_3)_2{\cdot}2H_2O$, 97%) obtained from Merck, 0.5 M sodium hydroxide (NaOH, 97%) obtained from Sigma Aldrich and 0.05 M dilute hydrochloric acid (HCl, 98%) obtained from Sigma Aldrich and indicator phenolphthalein (87 %) obtained from Sigma Aldrich.

2.2. Sample collection and identification

The samples of *Vigna unguiculata L* were collected in the Biological Garden of the Federal University Dutsin-Ma, Katsina, Nigeria. Plant specimens were identified, cleaned, dried, and authenticated at the Herbarium of the Department of Biological Sciences of the Federal University Dutsin-Ma. Then the mixture was ground to a fine powder and stored for further preparation and analysis. The structure of the *Vigna unguiculata* L. leaf is shown in Figure 1.

2.3. Preparation of Vigna unguiculata L. extract

The procedure reported by Rusman *et al.* [34] was adopted and modified for the present study. In this method, the *Vigna unguiculata* L. leaves were washed several times with deionized water to remove debris and dirt and then dried at room temperature for two weeks. The leaves were powdered using a blender and the powder with 100 meshes for a uniform size. The extract was prepared by adding 5.00 g of *Vigna unguiculata L* leaves powder in 100 mL of deionized water and stirred at 80 °C for 20 minutes. Subsequently, the mixture was filtered with Whatman No.1 filter paper, and then the filtrate was used for the synthesis of TiO_2-ZnO NC.

2.4. Synthesis of TiO_2-ZnO NCs

The procedure reported by Kelesoglu *et al.* [35] was adopted and modified for the present study. The co-precipitation method was used for the green synthesis of TiO_2-ZnO NCs with the solution prepared with 20 mL of *Vigna unguiculata L* extracts, 80 mL of deionized water, 5.93 g of zinc acetate dehydrate ($Zn(CH_3COO)_2{\cdot}2H_2O$) and 0.85 g of titanium acetate ($Ti(CH_3COO)_4$ as a precursor of ZnO and TiO_2 NPs, respectively. Then stirred at temperature 90 °C, constant speed at 500 rpm for 23 minutes and then homogenized for 5 minutes by constant stirring using a magnetic stirrer. Then sodium hydroxide (0.05M NaOH) was added dropwise to the solution until pH = 11. The paste was formed after continuous heating and stirring for overnight. The sample paste was evaporated at 80 °C for 10 hours and calcined at 650 °C for 2 hours using a muffle furnace to obtain TiO_2-ZnO NCs.

2.5. Determination of active sites

The amount of active sites of the TiO_2-ZnO NCs was studied using the back titration method. In back-titration analysis, the basicity of the base is reported as the acidity of the conjugate acid and vice versa. The TiO_2-ZnO NC catalyst was mixed with known concentration of HCl and will neutralize HCl concentration by an equivalent amount to its basicity. As a result, the original concentration of HCl will be reduced. The excess HCl will then be treated with a known concentration of NaOH and the amount of NaOH reacted is equivalent to the amount of basicity of the catalyst. Basicity measurement was carried out using mixed 0.2 mg of sample was stirred in 10 mL of distilled water and left for 24 h. The filtrate obtained was separated by centrifugation and the resulting solution was neutralized with 10 mL of 0.05 M HCl. Subsequently, the remaining acid was titrated with 0.05 M NaOH and phenolphthalein was used as an indicator [65]. Equation 1 relationship was used to determine the amounts of basic/acid sites from the recorded titre values.

$$\text{Active site (mmol/g)} = \frac{\text{Molarity of HCl reacted}}{\text{Mass of catalyst (g)}} \times 1000 \qquad (1)$$

2.6. Optimization

To find the optimum reaction conditions during the biosynthesis of TiO_2-ZnO NC from *Vigna unguiculata* L. extract, three levels and four variables of the Design Expert version thirteenth (DX13) of Box Behken Design (BBD) based on the response surface methodology (RSM) were used. The independent variables selected were the amount of dopant (A), reaction temperature (B), initial pH (C) and stirring time (D) while the other reaction variables such as the calcination temperature, amount of *Vigna unguiculata L* extract and the agitation speed were kept constant. As BBD is more accurate, more reliable, and less time consumption, there are three levels (low, central, and high corresponding to the coded levels -1, 0 and +1, respectively). These levels are displayed in Table 1 and a total of 29 sets of experiments were carried out according to the formula (N = 2n + 2n + 5, where n is the number of variables.

Table 2. RSM-BBD results with actual and predicted responses for the synthesis of TiO_2-ZnO NCs *.

Run	A	B	C	D	Actual active sites (mmol/g)	Predicted active sites (mmol/g)
1	5.00	90.00	8.00	20.00	8.71	9.17
2	1.00	90.00	4.00	20.00	8.67	8.71
3	5.00	90.00	8.00	20.00	9.65	9.21
4	5.00	90.00	4.00	15.00	8.89	8.08
5	5.00	85.00	4.00	20.00	8.56	8.20
6	5.00	95.00	8.00	15.00	9.67	9.46
7	10.00	85.00	4.00	15.00	8.67	8.74
8	1.00	85.00	8.00	20.00	8.76	8.78
9	5.00	90.00	11.00	15.00	8.59	8.60
10	5.00	90.00	11.00	30.00	8.98	9.06
11	5.00	90.00	8.00	20.00	9.54	9.78
12	5.00	90.00	8.00	20.00	7.11	7.73
13	10.00	90.00	4.00	20.00	9.67	9.62
14	10.00	90.00	8.00	30.00	5.98	7.32
15	5.00	90.00	8.00	20.00	8.67	8.27
16	5.00	85.00	11.00	20.00	8.98	9.97
17	5.00	95.00	4.00	20.00	7.45	9.05
18	10.00	90.00	11.00	20.00	8.67	7.61
19	5.00	95.00	8.00	30.00	8.98	9.05
20	1.00	90.00	8.00	30.00	9.11	9.18
21	1.00	90.00	11.00	20.00	7.87	8.54
22	10.00	95.00	8.00	20.00	8.98	9.12
23	1.00	95.00	8.00	20.00	8.65	9.35
24	5.00	85.00	8.00	30.00	8.45	8.79
25	5.00	85.00	8.00	20.00	9.34	8.79
26	1.00	90.00	8.00	15.00	6.89	8.79
27	10.00	90.00	8.00	15.00	8.99	8.16
28	5.00	95.00	11.00	15.00	8.98	8.79
29	5.00	90.00	4.00	30.00	9.11	8.98

* A is the amount of dopant (% MR TiO_2), B is the reaction temperature (°C), C is the initial pH and D is the stirring time (min).

The amount of active sites of the synthesized TiO_2-ZnO NCs obtained using Equation 1 was the experimental response (value). These data were processed using DX13 of the response surface methodology-box behnken design (RSM-BBD) to obtain the predicted value, response surface and regression model for the green synthesis of TiO_2-ZnO NCs.

2.7. Validation of models

The mathematical model developed by RSM-BBD for the amount of active site of TiO_2-ZnO NCs was validated and confirmed by experimenting with optimal conditions. The results were then compared with the predicted response. Each experiment was carried out in triplicate and the data was presented as mean±standard deviation (SD).

2.8. Simulated adsorption

Nitrogen adsorption isotherms at 77 K in optimized TiO_2-ZnO NCs were obtained with the Monte Carlo isobaric-isothermal Gibbs ensemble (NPT-GEMC) [66-69] as implemented in the Cassandra Monte Carlo (MC) simulation software [70,71]. Several force fields were used for optimized TiO_2-ZnO NCs. The transferable potential for the phase equilibrium force field (TraPPE) was used for nitrogen molecules [72]. Lorentz-Berthelot combining rules were employed to calculate the cross-interaction Lennard-Jones parameters. The equilibrium and production periods were performed for at least 5.0×10^6 MC steps each. Probabilities of translation, rotation, volume change, and particle swap between simulation boxes were included during MC simulations. The frameworks were fixed throughout the simulation [66].

2.9. Pore size distribution

The pore size distributions of the optimized TiO_2-ZnO NCs were determined using the NLDFT method. NLDFT pore size distributions (nldftPSD) were obtained via a demo version of SAIEUS software (www.nldft.com/dowload/) (Micromeritics, GA). The standard slit-pore mode for nitrogen adsorption at 77 K on carbon was selected because it is widely used in experiments to characterize nanomaterials. The L-curve method, which balances the roughness of the solution and the goodness of the fit, is implemented in SAIEUS when choosing λ as a user-adjustable parameter. The PSD result can be determined by solving an adsorption integral Equation 2 [69].

$$N_{exp}\left(\frac{P}{P_o}\right) = \int_{D_{min}}^{D_{max}} N_{NLDFT}\left(\frac{P}{P_o}\right) PSD(D)dD + \lambda \int_{D_{min}}^{D_{max}} [PSD^N(D)]^2\, dD \quad (2)$$

where λ is the chosen regularization (smoothing) parameter, N_{exp} is the experimental nitrogen adsorption at 77 K, N_{NLDFT}, represents the theoretical nitrogen adsorption isotherms assuming an ideal pore geometry such as a slit pore and cylindrical, PSD is the distribution of the pore size, P/P_0 is the pressure ratio with respect to the nitrogen saturation pressure and D is the pore diameter.

3. Results and discussion

3.1. Statistical analysis

3.1.1. Box Behnken experimental design

Four independent reaction conditions such as the amount of dopant, the reaction temperature, the initial pH and the stirring time were optimized by the response surface method (RSM) and the Box Behnken design (BBD) to determine the optimal conditions during the biosynthesis of TiO_2-ZnO NCs. A total of twenty- nine sets of design of experiments (DOE) were given by the design expert version-thirteen software. The twenty-nine set of experiments obtained from the response surface methodology –box Behnken design (RSM-BBD) was conducted and the amount of active site was calculated using Equation 1. Table 2 presents the experimental and predicted amounts of active sites in TiO_2-ZnO NCs during biosynthesis. The operational parameters, including dopant amount (A), reaction temperature (B), initial pH (C) and stirring time (D), are displayed in their actual levels.

Table 3. ANOVA for the response quadratic model

Source	Sum of square	DF	Mean square	F-value	*p*-value	Remarks
Model	11.16	14	1.12	3.03	0.0197	Significant
A	1.90	1	1.90	5.15	0.0033	-
B	0.28	1	0.28	0.75	0.0031	-
C	1.27	1	1.27	3.44	0.0011	-
D	0.015	1	0.015	0.042	0.0030	-
AB	0.11	1	0.11	0.30	0.0478	-
AC	0.85	1	0.85	2.30	0.0320	-
AD	1.59	1	1.59	4.31	0.0295	-
BC	4.00	1	4.00	10.86	0.0340	-
BD	0.78	1	0.78	2.13	0.0221	-
CD	0.37	1	0.37	1.01	0.0283	-
A^2	0.14	1	0.14	1.46	0.0560	-
B^2	0.56	1	0.56	1.36	0.0680	-
C^2	1.12	1	1.12	2.67	0.0466	-
D^2	1.34	1	1.34	2.56	0.0493	-
Residual	6.63	14	0.37	1.54	0.0489	-
Lack of fit	6.20	10	0.44	4.07	0.0924	Not significant
Pure error	0.43	4	0.11	-	-	-
Cor. total	17.79	28	-	-	-	-

Table 4. ANOVA of other important parameters for the response quadratic model.

Parameter	Value
Standard deviation	1.62
Mean	8.79
Correlation of variance (CV)	1.40
PRESS	20.59
Coefficient determined (R^2)	0.9272
Adjusted R^2	0.7546
Predicted R^2	0.9154
Adequate precision	6.0981

As seen from **Table 2** there was a close relationship between the actual (experimental) and predicted values. However, the closeness of the actual and predicted values is a primary indication of a true model [73]. Similarly, Table 2 also showed a good correlation between the actual and predicted amount of active sites ($mmolg^{-1}$) of TiO_2-ZnO NCs. The relationship between amount of active sites of TiO_2-ZnO NCs under the influence of the amount of dopant (A), temperature (B), initial pH (C) and stirring time (D) is explained by the quadratic model as given in terms of coded and actual factors according to Equations 3 and 4, respectively.

$$\text{Amount of basic active sites} = +8.79 + 0.56\,A + 0.80\,B + 0.90\,C + 0.69\,D - 0.17\,AB + 0.21\,AC - 0.63\,AD + 0.100\,BC - 0.29\,BD - 0.30\,CD \quad (3)$$

$$\text{Amount of basic active sites} = +8.79 + 0.56\,\text{amd} + 0.80\,\text{temp} + 0.90\,\text{pH} + 0.69\,\text{st} - 0.17\,\text{amd.temp} + 0.21\,\text{amd pH} - 0.63\,\text{amd st} + 0.100\,\text{temp pH} - 0.29\,\text{temp st} - 0.30\,\text{pH st} \quad (4)$$

The signs and values of the regression coefficients of the second-order polynomial model (Equations 3 and 4) represent the expected change in response per unit change in the value of independent variables used in the model. The sign of the coefficient of each operational parameter indicates its direction of change, while the coefficient values indicate the strength of the relationship. Therefore, the positive sign in front of the terms in the statistical Equations 3 and 4 shows a synergistic effect, which means an improvement in producing the amount of actives of the catalyst as opposed to the negative sign that shows an antagonistic effect [74,75]. In these Equations 3 and 4, the coefficient of one factor presented its effectiveness. To analyze the TiO_2-ZnO NCs amount of active sites through the coefficient values from the equations, it is clear that the initial pH gives a higher positive effect as compared to the operational parameters. The quality of the model was obtained by the analysis of variance (ANOVA), and its summary is presented in Table 3.

The model F-value of 3.03 implies that the model is significant and that there is only a 0.01 % chance that a model F value could occur due to some noise. The significance of the model terms is proven by the small *p*-value less than 0.0001. The *p*-values obtained range from 0.0011-0.0493 shows that all the model terms are significant. The most significant among the primary parameters were obtained as the initial pH (C) > reaction temperature (B) > stirring time (D) > amount of dopant (A) > reaction temperature-stirring time interaction (BD) > initial pH-stirring time interaction (CD) > amount of dopant-stirring time (AD) interaction > amount of dopant-initial pH (AC) interaction > temperature-initial pH (BC) interaction > amount of dopant-temperature interaction (AB) interaction > second-order initial pH (C^2)> second-order amount of dopant (A^2) >second-order stirring time (D^2) > seconder-reaction temperature (B2), respectively. Therefore, the initial pH (C) reaction temperature (B) were found to be the most significant operating variables for the biosynthesis of TiO_2-ZnO nanocomposites in comparison with the other selected process parameters. The 'lack of fit' value (LOF) is 4.07 and *p*-value is 0.0924 (more than 0.05), indicating good predictability of the model [76]. Furthermore, the other important statistical parameter for the response quadratic model is shown in Table 4.

According to Table 4, the standard deviation (SD = 1.62) and the coefficient of variance (CV = 1.40) are low demonstrating the high precision and good reliability of the experimental values. An adequate precision measure of 6.098 which is above 4 shows an adequate signal. The regression model explained a good relationship between independent variables as the coefficient of determination R^2 (0.9272) and predicted R^2_{pred} (0.9154) are closed to one. This shows good agreement between values predicted by the model and the values measured experimentally. To further analyze the appropriateness of the suggested models, diagnostic plots for both responses were studied. The adequacy of the regression model is explained as diagnostic plots. The diagnostic plots of both responses are presented in Figure 2.

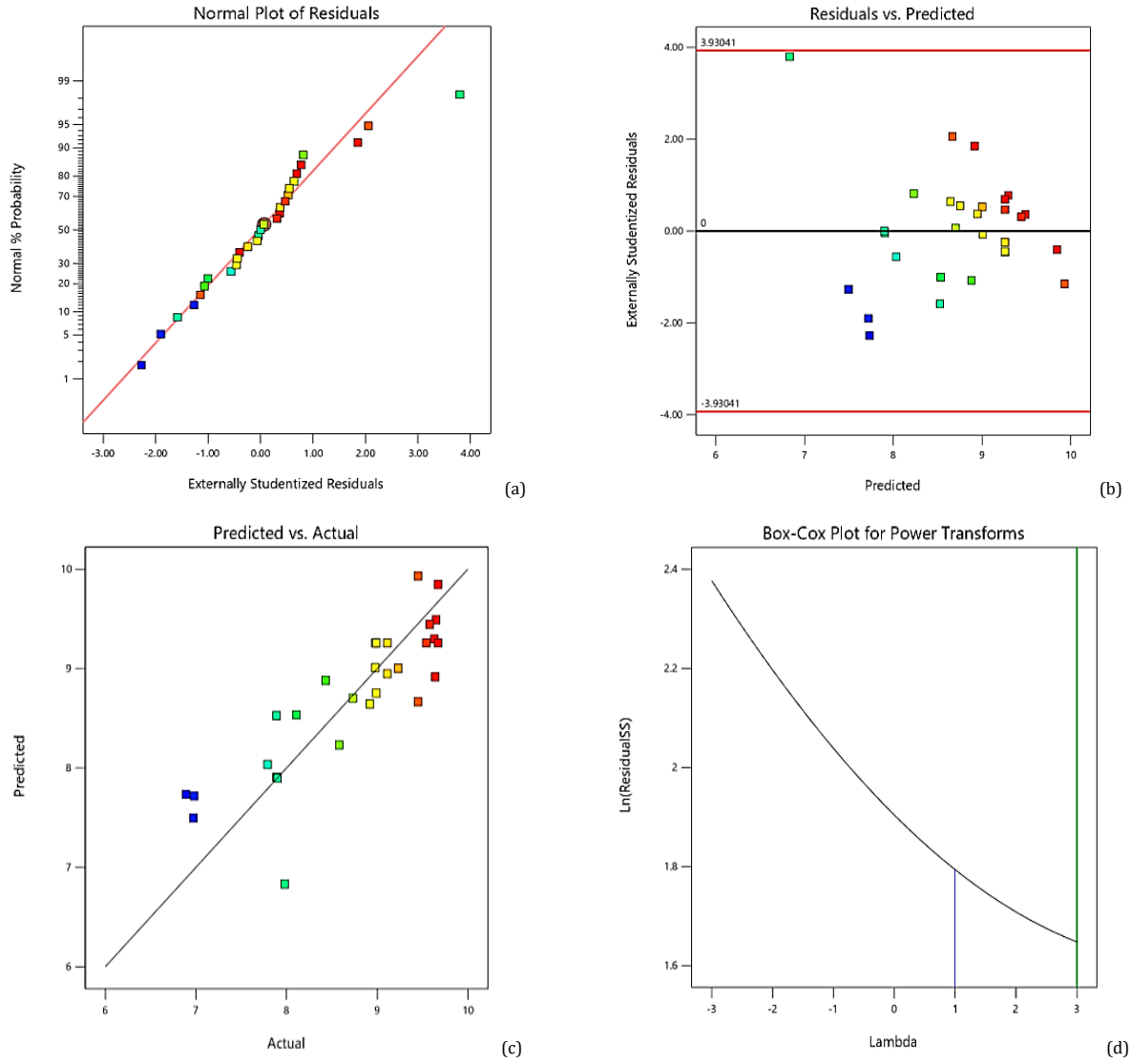

Figure 2. RSM diagnostic plots for (a) Normal plot of residuals, (b) Residuals *vs* predicted, (c) Predicted *vs* actual and (d) Box-Cox plot for power transforms.

Figure 2a shows the normal probability plot of externally studentized residuals. According to the graph, most of the point lies roughly on a straight line. This indicates that there is a close relationship between the actual and predicted values. Figure 2b illustrates the plot of the residuals and predicted. According to the graph, there is no obvious pattern, and the residuals are randomly distributed, implying that the model is sufficient. Figure 2c presents the plot of the actual and predicted values. Based on the graph, there is a uniform distribution of the points located in the center of the graph and a perpendicular line with a angle of 45° indicates the model's ability to predict the response appropriately. Figure 2d presents a Box-Cox plot for power transforms. These findings suggested that the models can significantly predict the effects of all factors on TiO_2-ZnO NC biosynthesis. Therefore, it can be concluded that the estimated effects are real and differ markedly from noise [76]. Due to the above-mentioned, the quality of the developed model is high and this implies that the amount of basic actives (8.881 mmol/g) of TiO_2-ZnO nanocomposites obtained during synthesis were influenced by the operating parameters within the studied range. Therefore, the above analysis of variance (ANOVA) shows that this predicted quadratic model is in good consistent with the experimental response and can be adopted.

3.2. Numerical parameter optimization

In this work, the response surface methodology optimization and modeling of green synthesis reaction conditions using *Vigna unguiculata L* extract were conducted. The four independent reaction conditions such as amount of dopant (1.00-10.00 %MR TiO2), the reaction temperature (85.00-95.00 °C), the initial pH (4.00-11.00) and the stirring time (15.00-30.00 min) were selected for optimization using RSM-BBD of the DX-13 software. However, 100 solutions were obtained with all having a desirability of one (1). But the first ten solutions were presented with the optimum amount of active sites (mmolg/L) of the TiO_2-ZnO NCs selected under optimal conditions during biosynthesis (Table 5).

The result presented in Table 3 demonstrates that the optimum amount of active sites (8.881 mmol/g) of the synthesized TiO_2-ZnO NCs was obtained at 10.00 % MR of TiO_2, 90 °C reaction temperature, initial pH of 11 and 23 min stirring time. However, the reaction conditions were in good agreement with the previous work reported [54]. Furthermore, the optimal conditions were further supported and confirmed by the solution ramps and the solution bar graph plots, as shown in Figure 3.

Table 5. Solutions of optimization of RSM-BBD of the green synthesis of TiO_2-ZnO NCs

Number	Amount of dopant	Temperature, °C	Initial pH	Stirring time, min	Active sites	Durability	Remark
1	10.00	90.00	11.00	22.50	8.881	1.00	Selected
2	10.00	90.00	7.50	30.00	8.665	1.00	-
3	10.00	95.00	7.50	22.50	8.790	1.00	-
4	10.00	85.00	7.50	22.50	8.039	1.00	-
5	10.00	90.00	4.00	22.50	7.496	1.00	-
6	10.00	90.00	7.50	15.00	8.644	1.00	-
7	10.00	89.49	10.36	17.15	8.940	1.00	-
8	10.00	87.59	5.40	15.68	7.079	1.00	-
9	10.00	93.21	4.67	28.72	8.515	1.00	-
10	10.00	85.06	8.78	15.80	8.046	1.00	-

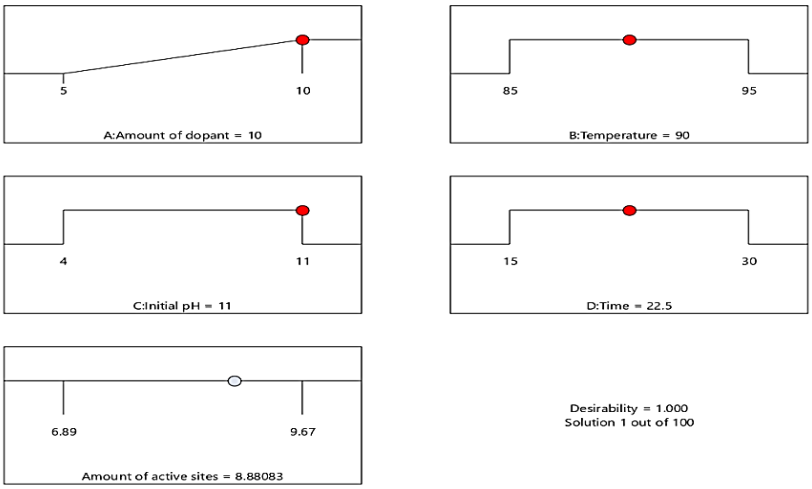

Figure 3. Ramp function plot for optimized parameters.

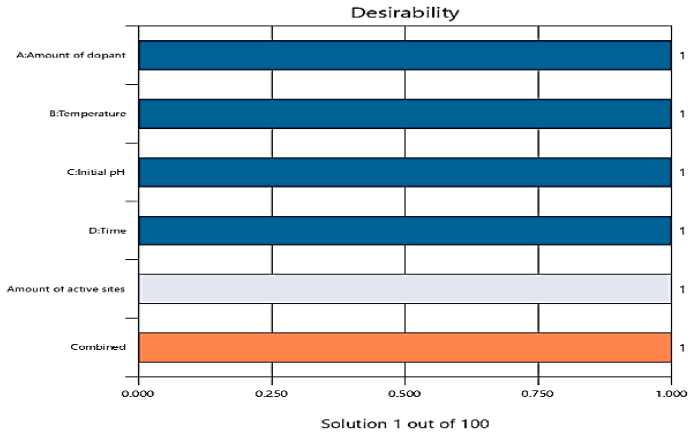

Figure 4. The bar graph for the solution.

Figure 3 shows the ranges for each of the operational parameters, their responses, and the optimum values selected by the RSM-BBD software. It can be seen that the amount of dopant ranges (1.00-10.00 % MR), and the optimal condition selected was found to be 10 % MR TiO_2, reaction temperature ranges (85-95 °C) and the optimal condition selected was found to be 90 ° C, initial pH ranges (4-11) and the optimum condition selected was found to be 11, stirring time ranges (15-30 min), and the optimum condition selected was approximately found to be 23 min and the amount of active sites ranges (6.89-9.67 mmol/g) and the optimum value selected was found to be 8.881 mmol/g.

3.3. Optimization using the desirability function

The influence of four selected reaction conditions; amount of dopant, reaction temperature, initial pH, and stirring time, on the biosynthesis of TiO_2-ZnO NCs was investigated using RSM-BBD of the DX13 software. The RSM method based on desirability functions explained by Derringer and Suich [77] was used to find the best combination of variables. However, in Table 5 and Figure 3, the optimal conditions for the biosynthesis of TiO_2-ZnO NCs were obtained with the desirability of each parameter. The desirability of the parameters of each individual process studied was found to be 1 (1.000) for the solution 1 out of 100. Therefore, the purpose of optimization using the desirability function is to find a combination of conditions for all parameters selected during the biosynthesis of TiO_2-ZnO NCs. Furthermore, the desirability for each of the selected reaction conditions and the desirability for the combined operating conditions is presented in Figure 4. The result displayed in Figure 4 illustrates the desirability of the individual operating parameter, the desirability of response, and the desirability of the combined process parameters for the solution ten (10.00) out of hundred (100.00).

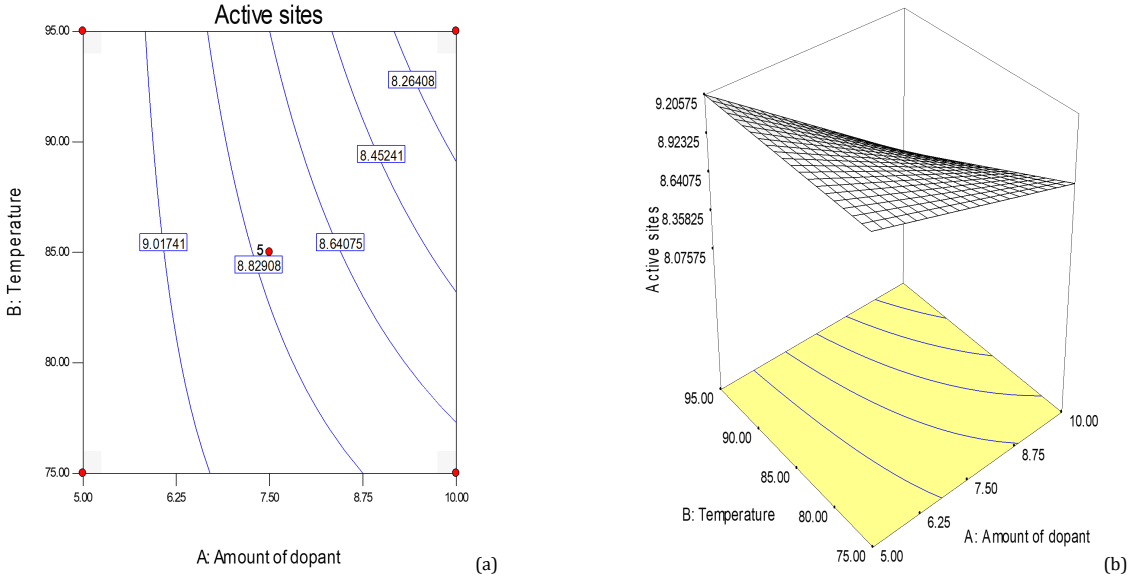

Figure 5. (a) 2D Contour plot and (b) 3D surface response plot for the interaction between the amount of dopant and reaction temperature.

According to the figure, the desirability of the amount of dopant (A) is one (1.00), desirability of reaction temperature (B) is 1.00, desirability of initial pH (C) is 1.00, desirability of stirring time (D) is 1.00, desirability of the response (amount of active sites) is 1.00 and desirability of combined operating parameters is also 1.00 respectively. This result clearly demonstrated that the desirability for all individual parameters, amount of active sites, and combined processes operating parameters were found to be equal to one for the solution of 10.00 out of 100.00. However, the same desirability value between the individual parameter, response, and combined processes operating variables is a primary indication for good optimal conditions. Therefore these findings, however,were consistent with the results presented in Table 5 and Figure 3, respectively.

3.4. Response surface analysis

The Response Surface Methodology-Box Behnken Design (RSM-BBD) analysis was carried out, and the results are presented using two-dimensional (2D) contour and three-dimensional (3D) surface response plots. A 3D surface response plot is the graphical representation of the regression equation obtained from the established model. However, the plots are based on the function of two variables, while the other operational variables are constant (under its optimum conditions). Furthermore, the elliptical or saddle shape of the contour plot specifies the level of significance of the interaction, and an elliptical or saddle plot will be obtained when there is a perfect interaction among independent variables [78,79].

3.4.1. Effect of the amount of dopant and reaction temperature

The interaction between the amount of dopant (A) and reaction tempertaure (B) plays a crucial role in determining the amount of active sites during the biosynthesis of TiO_2-ZnO NCs. The 2D contour and 3D surface response plots are shown in Figure 5. Figure 5a shows the 2D contour plot and the 3D surface response plot of the number of active sites for the TiO_2-ZnO NCs using the interaction between the amount of dopant and the reaction temperature. The red-colored region in the contour plot represents the maxima of the response surface plot. The optimal amount of active sites is predicted from the contour plot [39]. According to Figure 5, the number of active sites of TiO_2-ZnO NC decreased linearly with increases of the amount of dopant (1.00-10.00 % MR TiO_2) and increased progressively with increases in reaction temperature (85.00-90.00 ° C) to the optimal level (9.500 mmol/g). These might be due to the fact that the active surface of the catalyst was blocked with a higher amount of dopant, which might lead to the higher crystallite size, pore size, pore volume, and lower surface area and subsequently decreased the amount of active sites. On the contrary, the amount of active sites increased with an increase in reaction temperature as a result of increases in the surface area and decreases in the crystallite size, pore size, and pore volume. The optimal amount of actives (9.50 mmol/g) was obtained at a temperature of around 91.99 °C and a dopant amount of around 5.90 % MRTiO_2.

3.4.2. Effect of the amount of dopant and initial pH

The interaction effects of the amount of dopant (A) and initial pH (C) play an important role in determining the amount of active sites during the biosynthesis of TiO_2-ZnO NCs. The 2D contour and 3D surface response plots are depicted in Figure 6. Figure 6 illustrates the 2D contour plot and the 3D surface response plot of the number of active sites for the TiO_2-ZnO NCs using the interaction between the amount of dopant and the initial pH. The red-colored region in the contour plot represents the maximums of the response surface plot. The optimal number of active sites is predicted from the contour plot [39]. According to the figures, the number of active sites decreased linearly with increasing dopant amount from 1.00-10.00 % MR TiO_2 and increased progressively with increasing pH of the initial solution (4.00-11.00). This is because as the amount of dopant increases, the active surface of the catalyst would be blocked, which in turn decreased the amount of active sites. As the initial pH was adjusted to higher levels, more hydroxyl ions would be produced, which might lead to the formation of a higher amount of active sites. Therefore, the optimal amount of active sites (9.50 mmol/g) was achieved at around 5.00 % MR TiO_2 and at an initial pH of approximately 8.99.

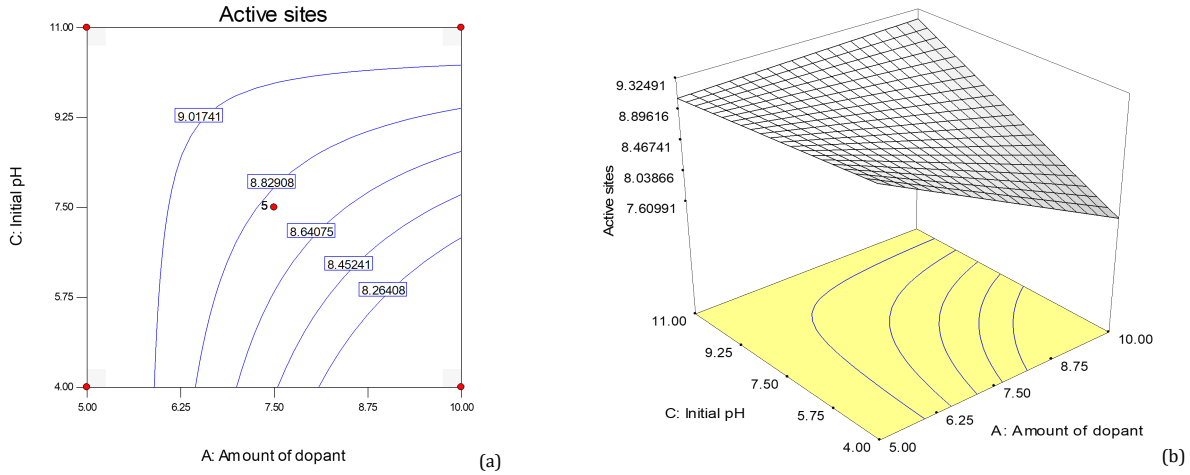

Figure 6. (a) 2D Contour plot and (b) 3D surface response plot for the interaction between the amount of dopant and the initial pH.

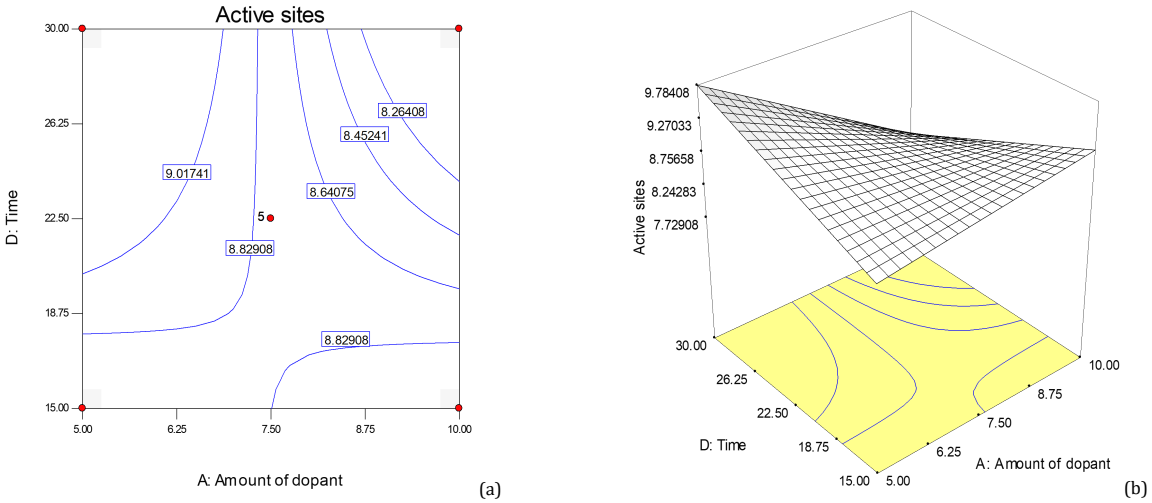

Figure 7. (a) 2D Contour plot and (b) 3D surface response plot for the interaction between the stirring time and the amount of dopant.

3.4.3. Effect of the stirring time and the amount of dopant

The interaction between the stirring time (D) and the amount of dopant (A) also plays a crucial role in determining the number of active sites during the biosynthesis of TiO_2-ZnO NCs. The 2D contour and 3D surface response plots are illustrated in Figure 7. Figure 7 indicates the 2D contour plot and the 3D surface response plot of the amount of active sites for the TiO_2-ZnO NCs using the interaction between the stirring time and the amount of dopant. The red-colored region in the contour plot represents the maxima of the response surface plot. The optimal amount of active sites is predicted from the contour plot [39]. According to the figures, the number of active sites decreased progressively as the amount of dopant increases from 1.00-10.00 % MR TiO_2 and decreased linearly with the increases of the stirring time from 15.00-30.00 min. This is because as the stirring time increases the crystal structure would be disturbed, in which the crystallite size would be increases and the surface area would decrease, which in turns decreases in the amount of active sites.

3.4.4. Effect of stirring time and initial pH

The interaction between the stirring time (D) and the initial pH (C) also plays a vital role in determining the number of active sites during the biosynthesis of TiO_2-ZnO NCs. The 2D contour and 3D surface response plots are presented in Figure 8. Figure 8 shows the 2D contour plot and the 3D surface response plot of the amount of active sites for the TiO_2-ZnO NCs using the interaction between the stirring time and the initial pH. The red-colored region in the contour plot represents the maximums of the response surface plot. The optimal number of active sites is predicted from the contour plot [39]. On the other hand, Figure 8 reveals that the number of active sites increased with increasing initial pH slowly from 4.00-6.50 and rapidly from 6.50-10.99. This indicates that the synthesized catalyst is basic in nature. The number of active sites increased progressively with increasing stirring time (15.00-25.11 min). These could be attributed to the fact that both the stirring time and the initial pH are important parameters for determining the amount of actives of the TiO_2-ZnO NCs during green synthesis. The optimal value for the amount of active sites (9.00 mmol/g) was obtained at the initial pH = 10.87 and 26.00 min stirring time, respectively. However, above the optimal conditions, the amount of active sites decreased with increases of the stirring time and with decreases in the initial pH.

3.4.5. Effect of reaction temperature and stirring time

The interaction between reaction temperature (B) and stirring time (D) also plays a wonderful role in determining the number of active sites during the biosynthesis of TiO_2-ZnO NCs. The 2D contour and 3D surface response graphs are presented in Figure 9.

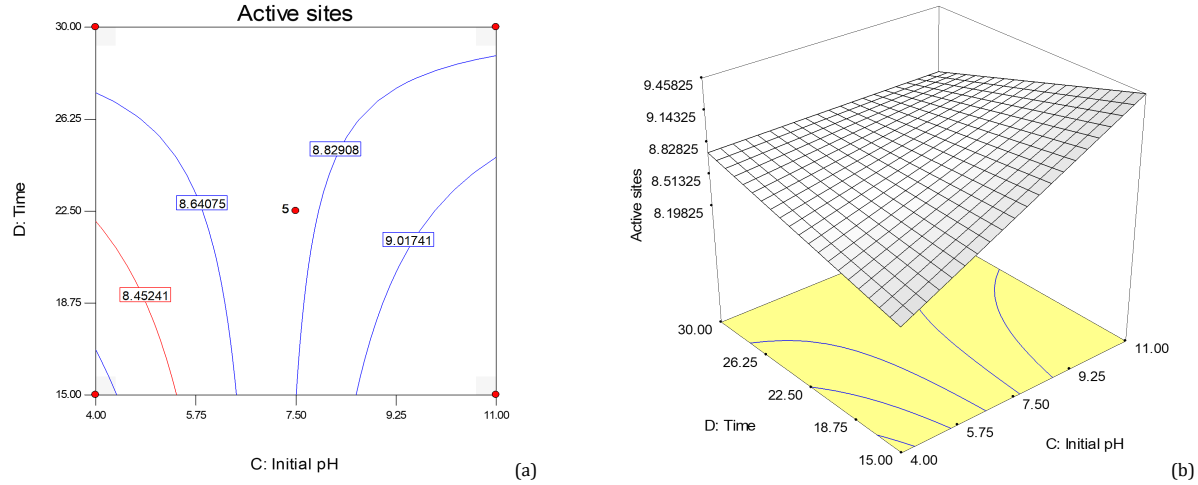

Figure 8. (a) 2D Contour plot and (b) 3D surface response plot for the interaction between the stirring time and the initial pH.

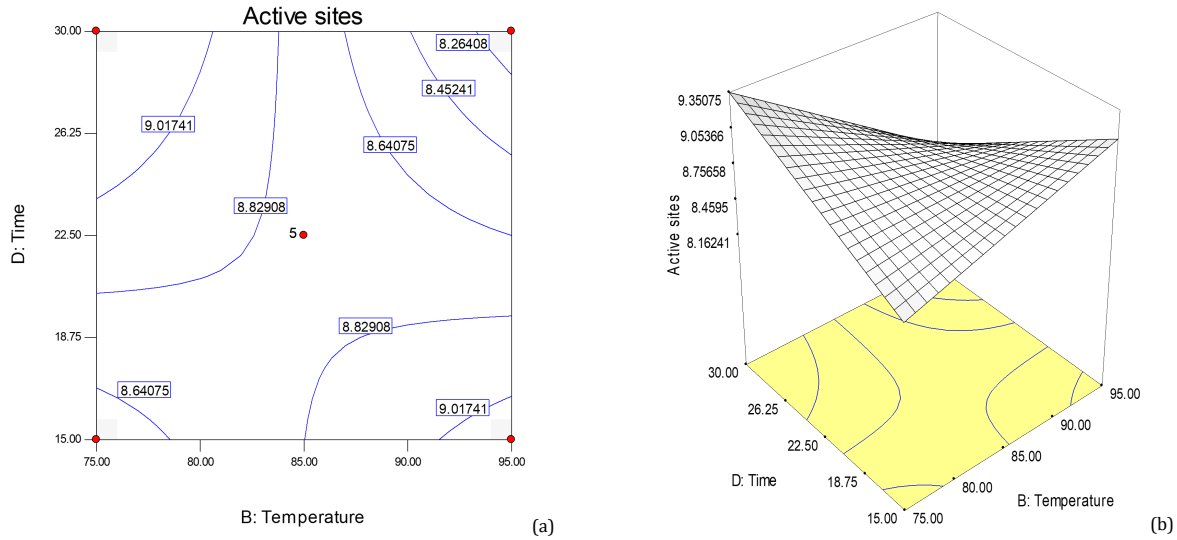

Figure 9. (a) 2D Contour plot and (b) 3D surface response plot for the interaction between the reaction temperature and the stirring time.

Figure 9 shows the 2D contour graph and the 3D surface response graph of the number of active sites for the TiO_2-ZnO NCs using the interaction between the reaction temperature and the stirring time. The red-colored region in the contour plot represents the maximums of the response surface plot. The optimal number of active sites is predicted from the contour plot [39]. According to the figures, the amount of active sites increased progressively with increasing reaction temperature from 85.00-95.00 °C and increased with increasing stirring time from 15.00-26.11 min. This might be attributed to the fact that, as the reaction temperature and stirring time increased, more surface area was produced and less crystallite size was produced, which in turn increased the active site of the catalyst. The optimal value for the amount of active sites (9.4 mmol/g) was obtained at around 91.80 °C and 26.75 min. Conversely, the amount of active sites decreased above the optimal stirring time condition with no significant effect on the reaction temperature.

3.4.6. Reaction temperature and initial pH

The interaction between reaction temperature (B) and initial pH (C) also plays a crucial role in determining the number of active sites during the biosynthesis of TiO_2-ZnO NCs. The 2D contour and 3D surface response plots are shown in Figure 10. Figure 10 illustrates the 2D contour plot and the 3D surface response plot of the amount of active sites for TiO_2-ZnO NCs using the interaction between the reaction temperature and the initial pH. The red-colored region in the contour plot represents the maximums of the response surface plot. The optimal number of active sites is predicted from the contour plot [39]. Based on the figures, the amount of active sites increased linearly with increases in the reaction temperature from 85.00-95.00 °C and increased progressively with the increases of initial pH from 4.00-11.00. These highlighted that both the temperature and the initial pH are essential variables for the determination of the active sites of TiO_2-ZnO NCs. The optimal predicted amount of active sites (9.00 mmol/g) was obtained at temperature of 95.00 °C and an initial pH of 8.11. Moreover, above optimal conditions, the amount of active sites decreased with increasing initial pH with no significant effect on the reaction temperature.

3.5. Optimization using the perturbation method

The interactions between the operational parameters can also be described using the perturbation method which came up by default from the design expert software and perturbation theory using mathematical methods for finding an optimized

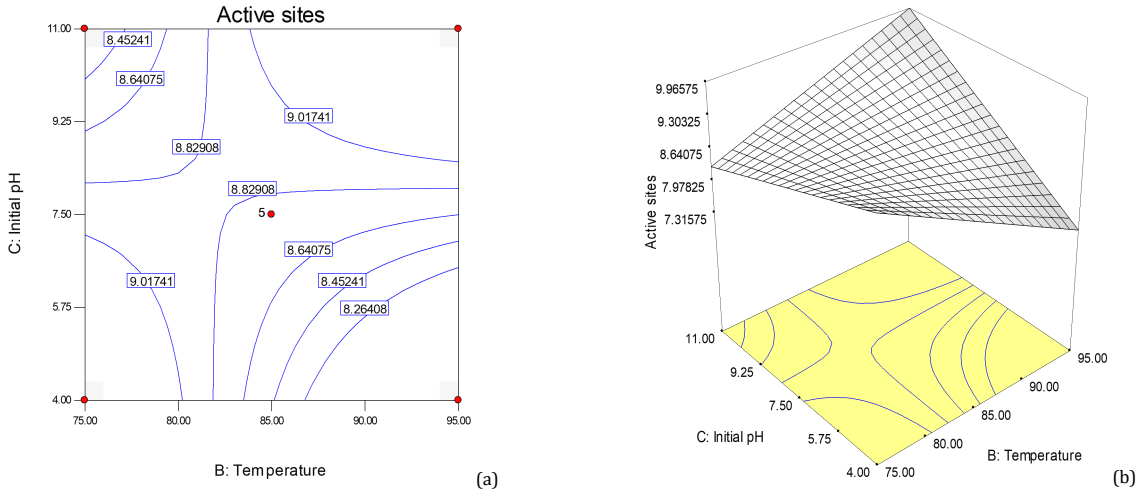

Figure 10. (a) 2D contour plot and (b) 3D surface response plot for the interaction between the reaction temperature and the initial pH.

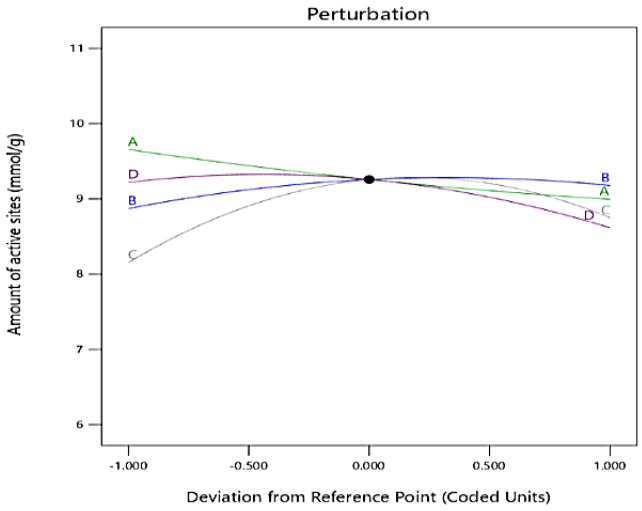

Figure 11. Perturbation plots for the number of active sites of TiO_2-ZnO NCs. (A: amount of dopant, B: reaction temperature, C: initial pH, and D: stirring time.

condition to the solve the problem. In this study, the influence of the variables studied individually, comprising the amount of dopant (A), reaction temperature (B), initial pH (C), and stirring time (D), on the amount of active sites of TiO_2-ZnO NCs as the response, was studied using perturbation plots. The perturbation plot utilizes the model terms to visualize the effect of each factor deviation from the reference point on the response. It can be used to explore the most significant factors in response. A steep slope or curvature of the graph reveals that the response is sensitive to that variable, whereas a relatively plane line indicates the insensitivity of the response to change in that particular factor [80]. Figure 11 shows the perturbation plot of the amount of active sites in the TiO_2-ZnO NC biosynthesis.

It can be seen in Figure 11; the initial pH curve displays a high steep curvature followed by the reaction temperature. However, the stirring time and amount of dopant curves show a low curvature indicating these factors have a slight effect on the response. These observations were confirmed from the coefficients of the model terms in Equation 3 and analysis of variance (ANOVA) (Table 3). Therefore, as observed from the ANOVA, regression model equation and perturbation plots, the most significant parameter that greatly contributed during the biosynthesis of TiO_2-ZnO NCs is the initial pH followed by the reaction temperature. On the basis of the above findings, the role of these wonderful parameters (initial pH and reaction temperature) was further described herein.

3.5.1. Effect of initial pH

One of the crucial parameters that play an important role as compared to the other selected conditions in the biosynthesis of nanoparticles (TiO_2-ZnO NCs) is the pH of the solution. It usually ranges from 1.00-14.00 on the pH scale [81]. The low values normally range (1.00-6.00) correspond to the acidic, and the moderate value (7.00) corresponds to the alkaline, while the high values range (8.00-14.00) correspond to the basic [82]. At low pH (below 5.00) an alternative to reduction oxidation occurred, while at a very high pH (above 9.00, 10.00) the reduction rate would be too high, resulting in the aggregation of TiO_2-ZnO NCs [83]. However, information from the literature demonstrated that nanoparticle synthesis was carried out at high pH because the reduction rate is high at high pH [84,85]. Similarly, the amount of active site (response) during the biosynthesis of TiO_2-ZnO NCs progressively increased from lower to higher pH values to optimal levels. This is because as the initial pH was adjusted to a higher level more hydroxyl ions would be produced, which might lead to the formation of a higher number of active sites [85]. Similarly, the developed model revealed the same explanations, since the optimum condition of the initial pH in the biosynthesis of TiO_2-ZnO NCs

Table 6. Confirmation data ANOVA of the quadratic model

Run	Amt of dop (MR % TiO_2)	Temperature (°C)	Initial pH	Precipitation time (min)	Actual (mmol/g)	Predicted (mmol/g)
1	1.00	75.00	4.00	15.00	7.68±0.35	7.980
2	5.00	85.00	8.00	20.00	8.67±0.15	8.740
3	10.00	95.00	11.00	30.00	8.89±0.02	8.906

Table 7. Comparison in this study with previously reported synthesized TiO_2-ZnO NCs in terms of method of synthesis, plant extract, optimization of reaction conditions, and applications.

Photocatalyst	Synthesized method	Type of extract	Optimization	Application	Reference
ZnO/TiO_2	Green synthesis	*Calopogonium mucunoides*	Not available	Treatment congo red dye	[34]
2-D fern-like ZnO/TiO_2	Green synthesis	*Hibiscus subdariffa*	Not available	Treatment of methylene blue dye	[88]
ZnO-TiO_2 nanohybrids	Hydrothermal	Not available	Not available	Treatment of methylene blue and methyl orange dyes	[89]
ZnO/TiO_2 composite	Sol gel	Not available	Not available	Treatment of methylene blue dye	[90]
ZnO/TiO_2	Solid state	Not available	Not available	Treatment of quinoline	[91]
TiO_2/ZnO composite sphere	Solvothermal	Not available	Not available	Treatment of rhodamine blue dye	[92]
ZnO/TiO_2 NCs	Pulsed laser ablation	Not available	Not available	Treatment of methyl orange dye	[93]
ZnO/TiO_2 NCs	Chemical method	Not available	Not available	Treatment of bentazon dye	[94]
ZnO/TiO_2 heterojunction	Mechanical mixing	Not available	Not available	Treatment of rhodamine B blue dye	[95]
ZnO/TiO_2 composite	Hydrothermal	Not available	Not available	Treatment of methylene blue and methyl orange dyes	[96]
ZnO/TiO_2 NCs	Sol gel and precipitation	Not available	Not available	Treatment of methyl orange dye	[97]
ZnO/TiO_2 Core/shell	Sol gel deposition	Not available	Not available	Treatment of methylene blue dye	[98]
ZnO/TiO_2 NCs	Hydrothermal	Not available	Not available	Treatment of methyl orange dye	[99]
ZnO/TiO_2 NCs	Electrostatistically modified electrospinning	Not available	Not available	Treatment of methyl orange dye	[100]
ZnO@TiO_2 NCs	Green synthesis	*Cinnamomum verum*	Not available	Surface characterization	[35]
ZnO/TiO_2 NCs	Green synthesis	*Hibiscus rosa-sinensis*	Not available	Treatment of bacteria	[101]
TiO_2-ZnO NCs	Green synthesis	*Vigna unguiculata* L	Available	Beneficial for the mesoporous materials community	Present

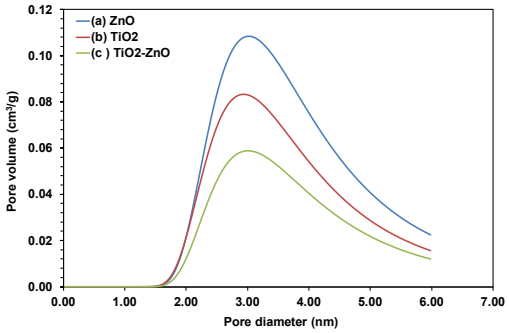

Figure 12. Particle size distributions (a) ZnO, (b) TiO_2 (c) TiO_2-ZnO NCs

was 11. This shows that the optimized TiO_2-ZnO NCs were basic. These findings are in good agreement with the many previous related works [86,87]. The regression expression (Equation 3), the perturbation plot, and ANOVA (Table 3) also supported the observations mentioned above about pH with the probability value (*p*-value) of 0.0011.

3.5.2. Effect of the reaction temperature

Reaction temperature is an important factor to consider during the biosynthesis of nanoparticles. As seen from the perturbation plot, the reaction temperature (B) was found for the second variable that influences the amount of active site during the biosynthesis of TiO_2-ZnO NCs. The amount of active sites increased linearly with the increase in reaction temperature. This is because as the temperature increases, the surface area of the TiO_2-ZnO NCs increased and the crystallite sites decreased, which could lead to increases in the amount of active sites of the TiO_2-ZnO NCs.

3.6. Model validation analysis

To confirm the validity of the quadratic model developed in this synthesis, three biosynthesis runs were individually performed in three replicates (Table 6) under low, central and high conditions of the independence variables selected for this study, and the result is presented in Table 6. The result obtained in Table 6 was compared with the predicted responses (Table 2). The experimental values were very close to the predicted values (8.88 mmol/g), confirming the reliability of the BBD.

3.7. Nonlinear density functional theory pore size distributions

The pore size, pore volume, pore size distributions (PSD), and specific surface area (SSA) of the synthesized TiO_2-ZnO NCs were determined using the nonlinear functional theory (NLDFT) method. The regularization parameters are selected using the L-curve method available in SAIEUS. SSA was found to be 190.04, 254.90 and 351.80 m^2/g for the ZnO, TiO_2 and TiO_2-ZnO NCs, respectively. The increase in SSA for TiO_2-ZnO NC could be due to the incorporation of TiO_2 on the surface of ZnO NP. On the other hand, the pore sizes were found to be 3.28, 3.24 and 3.23 nm for the ZnO, TiO_2 and TiO_2-ZnO NCs, respectively. The pore volumes were found to be 1.16×10^{-1}, 8.01×10^{-2} and 5.45×10^{-2} cm^3/g for the ZnO, TiO_2 and TiO_2-ZnO NCs, respectively. These results indicated that the higher the specific surface area, the lower the pore size and pore volume of the TiO_2-ZnO NCs and vice versa. These findings are in good agreement with many results presented in previous related

work [35]. The particle size distributions (PSD) of the ZnO, TiO_2, and TiO_2-ZnO NCs are presented in Figure 12. As seen in Figure 12, the pore sizes of all working catalysts are within the porosity range of 2.00-50 nm. Therefore, it can be concluded that the ZnO, TiO2, and TiO_2-ZnO NCs are mesoporous or mesopore in nature.

3.8. Comparative analysis

To show the novelty in this work, we have compared the method of preparation, type of plant extract, optimization during the synthesis, and applications of the synthesized TiO_2-ZnO NCs in this study with previous related work as shown in Table 7. It can be seen from Table 7 that the optimization of reactions in the biosynthesis of TiO_2-ZnO NCs from the *Vigna unguiculata* L. extract has not been reported in the previous works. Furthermore, synthesized TiO_2-ZnO NCs are beneficial to the mesoporous materials community because the validation of NLDFTPSD has been an extremely challenging task as a result of the experimentally indirect techniques used for such calculation.

4. Conclusions

TiO_2- ZnO NCs were prepared by green synthesis via the coprecipitation method from the *Vigna unguiculata L* extract as a reducing and stabilizing agent. Optimization of the reaction variables such as amount of dopant, reaction temperature, initial pH, and stirring time was conducted using response surface methodology box Behnken design of the DX13 software. The amount of active site of TiO_2-ZnO NCs was calculated using acid-base back titration analysis. The optimal amount of active site (8.881 mmol/g) archived at 10.00 % MR TiO_2, reaction temperature 90 °C, initial pH = 11 and stirring time 23 min. The regression model and the analysis of variance demonstrated that the most significant parameter that contributed enormously to the biosynthesis of TiO_2-ZnO NC was the initial pH. Similarly, the 3D and 2D contour plots also showed a good interaction between the two variables. Consequently, the perturbation analysis plot indicated that the initial pH, the stirring time, and the reaction temperature have a linear relation. The NLDFT specific surface area, pore size, and pore volume were found to be 351.80 m^2/g, 3.23 nm and 5.45×10^{-2} cm^3/g for TiO_2-ZnO NC, respectively. PSDs of TiO_2-ZnO NCs according to the NLDFT were found to be mesoporous in nature. Therefore, the synthesized TiO_2-ZnO NCs are beneficial for the mesoporous material community.

Acknowledgements

The authors acknowledge the effort of the Department of Chemistry Faculty of Physical Sciences of Federal University, Dutsin-Ma for providing most of the facilities during this research work.

Disclosure statement

Conflict of interest: The authors declare that they have no conflict of interest.
Ethical approval: All ethical guidelines have been adhered.
Sample availability: Samples of the compounds are available from the author.

CRediT authorship contribution statement

Conceptualization: Auwal Yusha'u; Methodology: Kamaluddeen Sulaiman Kabo; Software: Auwal Yusha'u; Validation: Siaka Abdulfatai Adabara; Formal Analysis: Kamaluddeen Sulaiman Kabo; Investigation: Auwal Yusha'u; Resources: Auwal Yusha'u; Data Curation: Siaka Abdulfatai Adabara; Writing - Original Draft: Auwal Yusha'u; Writing - Review and Editing: Kamaluddeen Sulaiman Kabo; Visualization: Siaka Abdulfatai Adabara; Funding acquisition: Auwal Yusha'u; Supervision: Kamaluddeen Sulaiman Kabo; Siaka Abdulfatai Adabara; Project Administration: Kamaluddeen Sulaiman Kabo.

ORCID and Email

Auwal Yusha'u
ayusha21@fudutsinma.edu.ng
auwalyushau2018@gmail.com
https://orcid.org/0000-0002-1713-9434
Kamaluddeen Sulaiman Kabo
kskabo@fudutsinma.edu.ng
https://orcid.org/0000-0003-4000-6901
Siaka Abdulfatai Adabara
asiaka@fudutsinma.edu.ng
https://orcid.og/0000-0001-8527-5780

References

[1]. Kumar, P. S. M. Francis, A. P.; Devasena, T. Biosynthesized and chemically synthesized Titania nanoparticles: Comparative analysis of antibacterial activity. *J. Environ. Nanotechnol.* **2014**, *3*, 73–81. https://doi.org/10.13074/jent.2014.09.143098
[2]. Robert, D.; Weber, J. V. Titanium Dioxide Synthesis by Sol Gel Methods and Evaluation of Their Photocatalytic Activity *J. Mater. Sci. Lett.* **1999**, *18*, 97–98. https://doi.org/10.1023/A:1006645930952
[3]. Chandra, A.; Bhattarai, A.; Yadav, A. K.; Adhikari, J.; Singh, M.; Giri, B. Green Synthesis of Silver Nanoparticles Using Tea Leaves from Three Different Elevations. *ChemistrySelect* **2020**, *5* (14), 4239–4246.
[4]. Syahin Firdaus Aziz Zamri, M.; Sapawe, N. Effect of pH on Phenol Degradation Using Green Synthesized Titanium Dioxide Nanoparticles. *Mater. Today: Proc.* **2019**, *19*, 1321–1326.
[5]. Kalyanasundaram, S.; Prakash, M. J. Biosynthesis and characterization of titanium dioxide nanoparticles using Pithecellobium Dulce and Lagenaria siceraria aqueous leaf extract and screening their free radical scavenging and antibacterial properties. *Int. Lett. Chem. Phys. Astron.* **2015**, *50*, 80–95.
[6]. Singh, J.; Dutta, T.; Kim, K.-H.; Rawat, M.; Samddar, P.; Kumar, P. "Green" synthesis of metals and their oxide nanoparticles: applications for environmental remediation. *J. Nanobiotechnology* **2018**, *16*, 84.
[7]. Singh, J.; Kumar, V.; Kim, K.; Rawat, M. Biogenic synthesis of copper oxide nanoparticles using plant extract and its prodigious potential for photocatalytic degradation of dyes. *Environ. Res.* **2019**, *177*, 108569.
[8]. Awad, M.; Farrag, A.; Aboelnga, M.; El-Bindary, A. Optimization of Photocatalytic Degradation of Rhodamine B and Indigo Carmine Dyes Using Eco-Friendly Kaolinite-Silver Oxide Quantum Dots Nanocomposite Under Sunlight Irradiation. *Applied Organom Chemis* **2024**, *39* (2), 7842 https://doi.org/10.1002/aoc.7842.
[9]. Singh, J.; Mehta, A.; Rawat, M.; Basu, S. Green synthesis of silver nanoparticles using sun dried tulsi leaves and its catalytic application for 4-Nitrophenol reduction. *J. Environ. Chem. Eng.* **2018**, *6* (1), 1468–1474.
[10]. Iravani, S. Green synthesis of metal nanoparticles using plants. *Green Chem.* **2011**, *13* (10), 2638–2650.
[11]. Shaker, S.; Mohsin, A. K.; edan, M. Preparation $Tio_2$and Zno/Tio_2nanocomposites locally and use against Staphylococcus aureus. *IOP. Conf. Ser.: Mater. Sci. Eng.* **2020**, *928* (7), 072014.
[12]. Mondal, K.; Sharma, A. Recent advances in the synthesis and application of photocatalytic metal–metal oxide core–shell nanoparticles for environmental remediation and their recycling process. *RSC. Adv.* **2016**, *6* (87), 83589–83612.
[13]. Verma, V.; Al-Dossari, M.; Singh, J.; Rawat, M.; Kordy, M. G.; Shaban, M. A Review on Green Synthesis of TiO2 NPs: Photocatalysis and Antimicrobial Applications. *Polymers* **2022**, *14* (7), 1444.
[14]. Khan, I.; Saeed, K.; Khan, I. Nanoparticles: Properties, applications and toxicities. *Arab. J. Chem.* **2019**, *12*, 908–931.
[15]. Gupta, S. M.; Tripathi, M. A review of TiO2 nanoparticles. *Chin. Sci. Bull.* **2011**, *56* (16), 1639–1657.
[16]. Nabi, G.; Qurat-ul-Aain, ; Khalid, N. R.; Tahir, M. B.; Rafique, M.; Rizwan, M.; Hussain, S.; Iqbal, T.; Majid, A. A Review on Novel Eco-Friendly Green Approach to Synthesis TiO2 Nanoparticles Using Different Extracts. *J. Inorg Organomet Polym* **2018**, *28* (4), 1552–1564.
[17]. Thakkar, K. N.; Mhatre, S. S.; Parikh, R. Y. Biological synthesis of metallic nanoparticles. *Nanomed.: Nanotechnol. Biol. Med.* **2010**, *6* (2), 257–262.
[18]. Mittal, A. K.; Chisti, Y.; Banerjee, U. C. Synthesis of metallic nanoparticles using plant extracts. *Biotechnol. Adv.* **2013**, *31* (2), 346–356.
[19]. Kashale, A. A.; Gattu, K. P.; Ghule, K.; Ingole, V. H.; Dhanayat, S.; Sharma, R.; Chang, J.; Ghule, A. V. Biomediated green synthesis of TiO2 nanoparticles for lithium ion battery application. *Compos. B: Eng.* **2016**, *99*, 297–304.
[20]. Sett, A.; Gadewar, M.; Sharma, P.; Deka, M.; Bora, U. Green synthesis of gold nanoparticles using aqueous extract of *Dillenia indica*. *Adv. Nat. Sci: Nanosci. Nanotechnol.* **2016**, *7* (2), 025005.

[21]. Santhoshkumar, T.; Rahuman, A. A.; Jayaseelan, C.; Rajakumar, G.; Marimuthu, S.; Kirthi, A. V.; Velayutham, K.; Thomas, J.; Venkatesan, J.; Kim, S. Green synthesis of titanium dioxide nanoparticles using Psidium guajava extract and its antibacterial and antioxidant properties. *Asian Pac. J. Trop. Med.* **2014**, *7* (12), 968–976.

[22]. Ziental, D.; Czarczynska-Goslinska, B.; Mlynarczyk, D. T.; Glowacka-Sobotta, A.; Stanisz, B.; Goslinski, T.; Sobotta, L. Titanium Dioxide Nanoparticles: Prospects and Applications in Medicine. *Nanomaterials* **2020**, *10* (2), 387.

[23]. Piccinno, F.; Gottschalk, F.; Seeger, S.; Nowack, B. Industrial production quantities and uses of ten engineered nanomaterials in Europe and the world. *J. Nanopart Res* **2012**, *14* (9), https://doi.org/10.1007/s11051–012–1109–9.

[24]. Sridevi, K. P.; Prasad, L. G.; Sangeetha, B.; Sivakumar, S. Structural and optical study of ZnO-TiO2 nanocomposites. *JOR.* **2022**, *18* (3), 453–464.

[25]. Hudlikar, M.; Joglekar, S.; Dhaygude, M.; Kodam, K. Green synthesis of TiO2 nanoparticles by using aqueous extract of Jatropha curcas L. latex. *Mater. Lett.* **2012**, *75*, 196–199.

[26]. Hunagund, S. M.; Desai, V. R.; Kadadevarmath, J. S.; Barretto, D. A.; Vootla, S.; Sidarai, A. H. Biogenic and chemogenic synthesis of TiO_2NPs via hydrothermal route and their antibacterial activities. *RSC. Adv.* **2016**, *6* (99), 97438–97444.

[27]. Sundrarajan, M.; Bama, K.; Bhavani, M.; Jegatheeswaran, S.; Ambika, S.; Sangili, A.; Nithya, P.; Sumathi, R. Obtaining titanium dioxide nanoparticles with spherical shape and antimicrobial properties using M. citrifolia leaves extract by hydrothermal method. *J. Photochem. Photobiol. B: Biol.* **2017**, *171*, 117–124. https://doi.org/10.1016/j.jphotobiol.2017.05.003

[28]. Naik, R.; Jones, S.; Murray, C.; McAuliffe, J.; Vaia, R.; Stone, M. Peptide Templates for Nanoparticle Synthesis Derived from Polymerase Chain Reaction-Driven Phage Display. *Adv Funct Materials* **2004**, *14* (1), 25–30.

[29]. Dobrucka R. Synthesis of titanium dioxide nanoparticles using Echinacea purpurea herba. *Iran. J. Pharm. Res. Spring*, **2017,** *16(2),* 753–759.

[30]. Khade, G. V.; Suwarnkar, M. B.; Gavade, N. L.; Garadkar, K. M. Green synthesis of TiO2 and its photocatalytic activity. *J. Mater Sci: Mater Electron* **2015**, *26* (5), 3309–3315.

[31]. Thamima, M.; Karuppuchamy, S. Biosynthesis of Titanium Dioxide and Zinc Oxide Nanoparticles from Natural Sources: A Review. *Adv Sci Engng Med* **2015**, *7* (1), 18–25.

[32]. Singh, J.; Kumar, S.; Rishikesh, ; Manna, A. K.; Soni, R. Fabrication of ZnO–TiO2 nanohybrids for rapid sunlight driven photodegradation of textile dyes and antibiotic residue molecules. *Opt. Mater.* **2020**, *107*, 110138.

[33]. Kharissova, O. V.; Dias, H. R.; Kharisov, B. I.; Pérez, B. O.; Pérez, V. M. The greener synthesis of nanoparticles. *Trends Biotechnol.* **2013**, *31* (4), 240–248.

[34]. Rusman, E.; Heryanto, H.; Fahri, A. N.; Rahmat, R.; Mutmainna, I.; Tahir, D. Green synthesis ZnO/TiO2 for high recyclability rapid sunlight photodegradation wastewater. *MRS Adv.* **2022**, *7*, 444–449.

[35]. Keleşoğlu, G. S.; Özdinçer, M.; Dalmaz, A.; Zenkin, K.; Durmuş, S. Green synthesis and structural characterization of ZnO nanoparticle and ZnO@TiO2 nanocomposite by Cinnamomum verum bark extract. *Turk. J. Anal. Chem.* **2023**, *5* (2), 118–123.

[36]. Haghighizadeh, A.; Aghababai Beni, A.; Haghmohammadi, M.; Adel, M. S.; Farshad, S. Green Synthesis of ZnO-TiO2 Nano-Photocatalyst Doped with Fe(III) Ions Using Bitter Olive Extract to Treat Textile Wastewater Containing Reactive Dyes. *Water Air Soil Pollut* **2023**, *234* (6), 200–220 https://doi.org/10.1007/s11270–023–06374–w.

[37]. Atiek, E.; Matebu, A.; Tsegaye, D.; Behailu, G.; Abebe, B. Green synthesis of TiO2/ZnO heterostructure using Urtica Smensis leaf extract for antibacterial activity. *Results Chem.* **2024**, *12*, 101880.

[38]. Bognár, S.; Putnik, P.; Šojić Merkulov, D. Sustainable Green Nanotechnologies for Innovative Purifications of Water: Synthesis of the Nanoparticles from Renewable Sources. *Nanomaterials* **2022**, *12* (2), 263.

[39]. Ibrahim, M. M.; Sani, H. R.; Yahuza, K. M.; Yusuf, A. H.; Bungudu, A. B. Response surface optimization and modeling of caffeine photocatalytic degradation using visible light responsive perovskite structured LaMnO3. *Eur. J. Chem.* **2021**, *12*, 289–298.

[40]. Deriase, S. F.; El-Salamony, R. A.; Amdeha, E.; Al-Sabagh, A. M. Statistical optimization of photocatalytic degradation process of methylene blue dye by SnO–TiO_2–AC composite using response surface methodology. *Env Prog and Sustain Energy* **2021**, *40* (5), e13639 https://doi.org/10.1002/ep.13639.

[41]. Yushau, A.; Gaya, U. Carbon-Tunable p-type ZnO Nanoparticles for Enhanced Photocatalytic Removal of Eriochrome Black T. *J. Phys. Chem. Funct. Mater.* **2023**, *6*, 1–17.

[42]. Muhammad, A.; Sulaiman Kabo, K.; Yushau, A. Visible Light Induced Photocatalytic Removal of Methylene Blue Using Cu-tunable p-type ZnO Nanoparticles. *J. Phys. Chem. Funct. Mater.* **2023**, *6*, 1–14.

[43]. Yusha'u, A.; Darma, M. S.; Isah, K. A. Sol-gel synthesis of ZnO nanoparticles for optmized photocatalytic degradation of eriochrome Black T under UV irradiation. *Alger. J. Eng. Technol.* **2023**, *8* (1), 117–130.

[44]. Yusha'u, A.; Siaka, A. A.; Sulaiman Kabo, K.; Muhammad, A. Manganese-Tunable p-type ZnO Nanoscale for Optimized Photocatalytic Degradation of Terasil Blue from Wastewater. *Res. Biotechnol. Environ. Sci.* **2022**, *2* (4), 88–101.

[45]. Ghorbani, F.; Gorji, P.; Mobarakeh, M. S.; Mozaffari, H. R.; Masaeli, R.; Safaei, M. Optimized Synthesis of Xanthan gum/ZnO/TiO_2Nanocomposite with High Antifungal Activity against Pathogenic *Candida albicans*. *J. Nanomater.* **2022**, *2022* (1), https://doi.org/10.1155/2022/7255181.

[46]. Rajakumar, G.; Rahuman, A. A.; Priyamvada, B.; Khanna, V. G.; Kumar, D. K.; Sujin, P. Eclipta prostrata leaf aqueous extract mediated synthesis of titanium dioxide nanoparticles. *Mater. Lett.* **2012**, *68*, 115–117.

[47]. Gadore, V.; Singh, A. K.; Mishra, S. R.; Ahmaruzzaman, M. RSM approach for process optimization of the photodegradation of congo red by a novel NiCo2S4/chitosan photocatalyst. *Sci. Rep.* **2024**, *14*, 1118.

[48]. Lee, S. Y.; Kang, D.; Jeong, S.; Do, H. T.; Kim, J. H. Photocatalytic Degradation of Rhodamine B Dye by TiO2 and Gold Nanoparticles Supported on a Floating Porous Polydimethylsiloxane Sponge under Ultraviolet and Visible Light Irradiation. *ACS Omega* **2020**, *5* (8), 4233–4241.

[49]. Sani, K. I.; Gaya, U.; Hamisu, A. Synthesis of visible light response S-SnO2 catalyst for optimized photodegradation of bromophenol blue. *J. Phys. Chem. Funct. Mater.* **2021**, *4*, 22–33.

[50]. Dihom, H.; Mohamed, R. M. S. R.; Al-Gheethi, A.; Mohamed, W. A. B. W. Optimization and modeling of solar photocatalytic degradation of raw textile wastewater dyes using green ZnO-ED NPs by RSM. *Water Pract. Technol.* **2024**, *19*, 2279–2305.

[51]. Es-haghi, A.; Taghavizadeh Yazdi, M. E.; Sharifalhoseini, M.; Baghani, M.; Yousefi, E.; Rahdar, A.; Baino, F. Application of Response Surface Methodology for Optimizing the Therapeutic Activity of ZnO Nanoparticles Biosynthesized from Aspergillus niger. *Biomimetics* **2021**, *6* (2), 34. https://doi.org/10.3390/biomimetics6020034

[52]. Dhandapani, P.; Maruthamuthu, S.; Rajagopal, G. Bio-mediated synthesis of TiO2 nanoparticles and its photocatalytic effect on aquatic biofilm. *J. Photochem. Photobiol. B: Biol.* **2012**, *110*, 43–49.

[53]. Akerdi, A. G.; Bahrami, S. H.; Pajootan, E. Modeling and optimization of Photocatalytic Decolorization of binary dye solution using graphite electrode modified with Graphene oxide and TiO2. *J. Environ Health Sci Engineer* **2020**, *18* (1), 51–62.

[54]. Rakhmanova, A.; Kalybekkyzy, S.; Soltabayev, B.; Bissenbay, A.; Kassenova, N.; Bakenov, Z.; Mentbayeva, A. Application of Response Surface Methodology for Optimization of Nanosized Zinc Oxide Synthesis Conditions by Electrospinning Technique. *Nanomaterials* **2022**, *12* (10), 1733.

[55]. Mohd Yusof, H.; Abdul Rahman, N.; Mohamad, R.; Zaidan, U. H.; Samsudin, A. A. Optimization of biosynthesis zinc oxide nanoparticles: Desirability-function based response surface methodology, physicochemical characteristics, and its antioxidant properties. *OpenNano* **2022**, *8*, 100106.

[56]. Mazloom, F.; Masjedi-Arani, M.; Ghiyasiyan-Arani, M.; Salavati-Niasari, M. Novel sodium dodecyl sulfate-assisted synthesis of Zn3V2O8 nanostructures via a simple route. *J. Mol. Liq.* **2016**, *214*, 46–53.

[57]. Ghaedi, M.; Ghaedi, A.; Mirtamizdoust, B.; Agarwal, S.; Gupta, V. K. Simple and facile sonochemical synthesis of lead oxide nanoparticles loaded activated carbon and its application for methyl orange removal from aqueous phase. *J. Mol. Liq.* **2016**, *213*, 48–57.

[58]. Shaterian, M.; Enhessari, M.; Rabbani, D.; Asghari, M.; Salavati-Niasari, M. Synthesis, characterization and photocatalytic activity of LaMnO3 nanoparticles. *Appl. Surf. Sci.* **2014**, *318*, 213–217.

[59]. Raja, P.; Bensimon, M.; Kulik, A.; Foschia, R.; Laub, D.; Albers, P.; Renganathan, R.; Kiwi, J. Dynamics and characterization of an innovative Raschig rings–TiO2 composite photocatalyst. *J. Mol. Catal. A: Chem.* **2005**, *237* (1-2), 215–223.

[60]. Han, D.; Sun, J.; Ge, J.; Wang, C.; Hu, P.; Liu, Y. Cross-linked proton exchange membrane covalently bonded with silicotungstic acid for enhanced proton conductivity. *Int. J. Hydrog. Energy* **2024**, *90*, 1300–1312. https://doi.org/10.1016/j.ijhydene.2024.10.175.

[61]. Safardoust-Hojaghan, H.; Salavati-Niasari, M.; Amiri, O.; Hassanpour, M. Preparation of highly luminescent nitrogen doped graphene quantum dots and their application as a probe for detection of Staphylococcus aureus and E. coli. *J. Mol. Liq.* **2017**, *241*, 1114–1119.

[62]. Diez-Orejas, R.; Feito, M. J.; Cicuéndez, M.; Casarrubios, L.; Rojo, J. M.; Portolés, M. T. Graphene oxide nanosheets increase Candida albicans killing by pro-inflammatory and reparative peritoneal macrophages. *Colloids Surf. B: Biointerfaces* **2018**, *171*, 250–259.

[63]. Abdu, M.; Tibebu, S.; Babaee, S.; Worku, A.; Msagati, T. A.; Nure, J. F. Optimization of photocatalytic degradation of Eriochrome Black T from aqueous solution using TiO2-biochar composite. *Results Eng.* **2025**, *25*, 104036.

[64]. Sugiyama, T.; Dabwan, A. H.; Katsumata, H.; Suzuki, T.; Kaneco, S. Optimization of Conditions for the Photocatalytic Degradation of

EDTA in Aqueous Solution with Fe-Doped Titanium Dioxide. *OJINM.* **2014**, *04* (03), 28–34.
[65]. Yacob, A. R.; Kabo, K. S. Effect of Calcination on the Basic Strength of Surface Modified Nano-Zinc Oxide Characterised by FTIR and Back Titration Methods. *AMR.* **2015**, *1107*, 326–332.
[66]. Mcgrother, S. C.; Gubbins, K. E. Constant pressure Gibbs ensemble Monte Carlo simulations of adsorption into narrow pores. *Mol. Phys.* **1999**, *97* (8), 955–965.
[67]. Panagiotopoulos, A. Z. Direct determination of phase coexistence properties of fluids by Monte Carlo simulation in a new ensemble. *Mol. Phys.* **1987**, *61* (4), 813–826.
[68]. Panagiotopoulos, A.; Quirke, N.; Stapleton, M.; Tildesley, D. Phase equilibria by simulation in the Gibbs ensemble. *Mol. Phys.* **1988**, *63* (4), 527–545.
[69]. Kupgan, G.; Liyana-Arachchi, T. P.; Colina, C. M. NLDFT Pore Size Distribution in Amorphous Microporous Materials. *Langmuir* **2017**, *33* (42), 11138–11145.
[70]. Shah, J. K.; Maginn, E. J. A general and efficient Monte Carlo method for sampling intramolecular degrees of freedom of branched and cyclic molecules. *J. Chem. Phys.* **2011**, *135* (13), 134121 https://doi.org/10.1063/1.3644939.
[71]. Shah, J. K.; Marin-Rimoldi, E.; Mullen, R. G.; Keene, B. P.; Khan, S.; Paluch, A. S.; Rai, N.; Romanielo, L. L.; Rosch, T. W.; Yoo, B.; Maginn, E. J. Cassandra: An open source Monte Carlo package for molecular simulation. *J. Comput Chem* **2017**, *38* (19), 1727–1739.
[72]. Potoff, J. J.; Siepmann, J. I. Vapor–liquid equilibria of mixtures containing alkanes, carbon dioxide, and nitrogen. *AIChE J.* **2001**, *47* (7), 1676–1682.
[73]. Meena, P. L.; Surela, A. K.; Chhachhia, L. K.; Meena, J.; Meena, R. Investigation of the photocatalytic potential of C/N-co-doped ZnO nanorods produced *via* a mechano-thermal process. *Nanoscale Adv.* **2025**, *7* (5), 1335–1352.
[74]. Tien, N. T.; Huyen, T. T.; Hien, L. P.; Huy, N. N. A study on the optimization of photocatalytic removal of enrofloxacin using TiO_2 material. *IOP. Conf. Ser.: Earth Environ. Sci.* **2021**, *652* (1), 012010.
[75]. Yusuff, A. S.; Olateju, I. I.; Adesina, O. A. TiO2/anthill clay as a heterogeneous catalyst for solar photocatalytic degradation of textile wastewater: Catalyst characterization and optimization studies. *Materialia* **2019**, *8*, 100484.
[76]. Chaker, H.; Ameur, N.; Saidi-Bendahou, K.; Djennas, M.; Fourmentin, S. Modeling and Box-Behnken design optimization of photocatalytic parameters for efficient removal of dye by lanthanum-doped mesoporous TiO2. *J. Environ. Chem. Eng.* **2021**, *9*, 104584.
[77]. Derringer, G.; Suich, R. Simultaneous Optimization of Several Response Variables. *J. Qual. Technol.* **1980**, *12* (4), 214–219.
[78]. Abd El-Kader, M. F. H.; Elabbasy, M. T.; Adeboye, A. A.; Zeariya, M. G. M.; Menazea, A. A. Morphological, structural and antibacterial behavior of eco-friendly of ZnO/TiO2 nanocomposite synthesized via Hibiscus rosa-sinensis extract. *J. Mater. Res. Technol.* **2021**, *15*, 2213–2220.
[79]. Munguti, L.; Dejene, F. Influence of annealing temperature on structural, optical and photocatalytic properties of ZnO–TiO2 composites for application in dye removal in water. *Nano-struct. Nano-Objects* **2020**, *24*, 100594.
[80]. Jawad, A. H.; Alkarkhi, A. F.; Mubarak, N. S. Photocatalytic decolorization of methylene blue by an immobilized TiO2 film under visible light irradiation: optimization using response surface methodology (RSM). *Desalin. Water Treat.* **2015**, *56* (1), 161–172.
[81]. Gherbi, B.; Laouini, S. E.; Meneceur, S.; Bouafia, A.; Hemmami, H.; Tedjani, M. L.; Thiripuranathar, G.; Barhoum, A.; Menaa, F. Effect of pH Value on the Bandgap Energy and Particles Size for Biosynthesis of ZnO Nanoparticles: Efficiency for Photocatalytic Adsorption of Methyl Orange. *Sustainability* **2022**, *14* (18), 11300.
[82]. Singh, M.; Sinha, I.; Mandal, R. Role of pH in the green synthesis of silver nanoparticles. *Mater. Lett.* **2009**, *63* (3-4), 425–427.
[83]. Anigol, L. B.; Sajjan, V. P.; Gurubasavaraj, P. M.; Ganachari, S. V.; Patil, D. Study on the effect of pH on the biosynthesis of silver nanoparticles using Capparis moonii fruit extract: their applications in anticancer activity, biocompatibility and photocatalytic degradation. *Chem. Pap.* **2023**, *77* (6), 3327–3345.
[84]. Handayani, W.; Ningrum, A. S.; Imawan, C. The Role of pH in Synthesis Silver Nanoparticles Using Pometia pinnata (Matoa) Leaves Extract as Bioreductor. *J. Phys.: Conf. Ser.* **2020**, *1428* (1), 012021.
[85]. Cervantes-Gaxiola, M.; Vázquez-González, F.; Rios-Iribe, E.; Méndez-Herrera, P.; Leyva, C. Effect of pH on the green synthesis of ZnO nanoparticles using Sorghum bicolor seed extract and their application in photocatalytic dye degradation. *Mater. Lett.* **2024**, *372*, 136982.
[86]. Miranda, A.; Akpobolokemi, T.; Chung, E.; Ren, G.; Raimi-Abraham, B. T. PH alteration in plant-mediated green synthesis and its resultant impact on antimicrobial properties of silver nanoparticles (AgNPs). *Antibiotics (Basel)* **2022**, *11*, 1592.
[87]. Traiwatcharanon, P.; Timsorn, K.; Wongchoosuk, C. Effect of pH on the Green Synthesis of Silver Nanoparticles through Reduction with Pistiastratiotes L. Extract. *AMR.* **2015**, *1131*, 223–226.
[88]. Suganthi, N.; Thangavel, S.; Kannan, K. Hibiscus subdariffa leaf extract mediated 2-D fern-like ZnO/TiO2 hierarchical nanoleaf for photocatalytic degradation. *FlatChem* **2020**, *24*, 100197.
[89]. Singh, J.; Kumar, S.; Rishikesh; Manna, A. K.; Soni, R. Fabrication of ZnO–TiO2 nanohybrids for rapid sunlight driven photodegradation of textile dyes and antibiotic residue molecules. *Opt. Mater.* **2020**, *107*, 110138.
[90]. Munguti, L.; Dejene, F. Influence of annealing temperature on structural, optical and photocatalytic properties of ZnO–TiO2 composites for application in dye removal in water. *Nano-Struct. amp; Nano-Objects* **2020**, *24*, 100594.
[91]. Gupta, D.; Chauhan, R.; Kumar, N.; Singh, V.; Srivastava, V. C.; Mohanty, P.; Mandal, T. K. Enhancing photocatalytic degradation of quinoline by ZnO:TiO2 mixed oxide: Optimization of operating parameters and mechanistic study. *J. Environ. Manag.* **2020**, *258*, 110032.
[92]. Pan, L.; Shen, G.-Q.; Zhang, J.-W.; Wei, X.-C.; Wang, L.; Zou, J.-J.; Zhang, X. TiO2–ZnO composite sphere decorated with ZnO clusters for effective charge isolation in photocatalysis. *Ind. Eng. Chem. Res.* **2015**, *54*, 7226–7232.
[93]. Gondal, M. A.; Ilyas, A. M.; Baig, U. Pulsed laser ablation in liquid synthesis of ZnO/TiO 2 nanocomposite catalyst with enhanced photovoltaic and photocatalytic performance. *Ceram. Int.* **2016**, *42*, 13151–13160.
[94]. Gholami, M.; Shirzad-Siboni, M.; Farzadkia, M.; Yang, J. Synthesis, characterization, and application of ZnO/TiO2 nanocomposite for photocatalysis of a herbicide (Bentazon). *Desalin. Water Treat.* **2016**, *57* (29), 13632–13644.
[95]. Sun, W.; Meng, S.; Zhang, S.; Zheng, X.; Ye, X.; Fu, X.; Chen, S. Insight into the transfer mechanisms of photogenerated carriers for heterojunction photocatalysts with the analogous positions of valence band and conduction band: A case study of ZnO/TiO2. *J. Phys. Chem. C Nanomater. Interfaces* **2018**, *122*, 15409–15420.
[96]. Das, A.; Kumar, P. M.; Bhagavathiachari, M.; Nair, R. G. Hierarchical ZnO-TiO2 nanoheterojunction: A strategy driven approach to boost the photocatalytic performance through the synergy of improved surface area and interfacial charge transport. *Appl. Surf. Sci.* **2020**, *534*, 147321.
[97]. El Mragui, A.; Daou, I.; Zegaoui, O. Influence of the preparation method and ZnO/(ZnO + TiO2) weight ratio on the physicochemical and photocatalytic properties of ZnO-TiO2 nanomaterials. *Catal. Today* **2019**, *321-322*, 41–51.
[98]. Kwiatkowski, M.; Chassagnon, R.; Heintz, O.; Geoffroy, N.; Skompska, M.; Bezverkhyy, I. Improvement of photocatalytic and photoelectrochemical activity of ZnO/TiO2 core/shell system through additional calcination: Insight into the mechanism. *Appl. Catal. B: Environ.* **2017**, *204*, 200–208.
[99]. Li, X.; Wang, C.; Xia, N.; Jiang, M.; Liu, R.; Huang, J.; Li, Q.; Luo, Z.; Liu, L.; Xu, W.; Fang, D. Novel ZnO-TiO 2 nanocomposite arrays on Ti fabric for enhanced photocatalytic application. *J. Mol. Struct.* **2017**, *1148*, 347–355.
[100]. Ramos, P. G.; Flores, E.; Sánchez, L. A.; Candal, R. J.; Hojamberdiev, M.; Estrada, W.; Rodriguez, J. Enhanced photoelectrochemical performance and photocatalytic activity of ZnO/TiO 2 nanostructures fabricated by an electrostatically modified electrospinning. *Appl. Surf. Sci.* **2017**, *426*, 844–851.
[101]. Abd El-Kader, M.; Elabbasy, M.; Adeboye, A. A.; Zeariya, M. G.; Menazea, A. Morphological, structural and antibacterial behavior of eco-friendly of ZnO/TiO2 nanocomposite synthesized via Hibiscus rosa-sinensis extract. *J. Mater. Res. Technol.* **2021**, *15*, 2213–2220.